

# Impurity states in antiferromagnetic Iron Arsenides

Qiang Han

Department of Physics, Renmin University, Beijing, China

Z. D. Wang

Department of Physics and Center of Theoretical and Computational Physics,  
The University of Hong Kong, Pokfulam Road, Hong Kong, China

(dated: September 4, 2008)

We explore theoretically impurity states in the antiferromagnetic spin-density wave state of the iron arsenide. Two types of impurity models are employed: one has only the intraband scattering while the other has both the intraband and interband scattering with the equal strength. Interestingly, the impurity bound state is revealed around the impurity site in the energy gap for both models. However, the impurity state is doubly degenerate with respect to spin for the first case; while the single impurity state is observed in either the spin-up or spin-down channel for the second one. The impurity-induced variations of the local density of states are also examined.

PACS numbers: 71.55.-i, 75.30.Fv, 75.10.Lp

The recent discovery of iron-based superconductors [1] has triggered intensive efforts to unveil the nature of and interplay between magnetism and superconductivity in this family of materials. Series of iron arsenide have been synthesized, which possess many similar features of the normal and superconducting states. Experimental measurements have reported that the undoped  $\text{ReFeAsO}$  (where  $\text{Re}$  = rare-earth metals) and  $\text{AFe}_2\text{As}_2$  (where  $\text{A}$  = divalent metals such as  $\text{Ba}$ ,  $\text{Ca}$ ,  $\text{Sr}$ ) compounds exhibit a long-range antiferromagnetic spin-density-wave (SDW) order [2, 3, 4, 5, 6, 7]. Upon electron/hole doping the SDW phase is suppressed and superconductivity emerges with  $T_c$  up to above 50 K [8, 9, 10, 11, 12].

At present, there is likely certain controversy on the understanding of the SDW state of the undoped FeAs-based parent compounds. Two kinds of theories have been put forward: 1) the itinerant antiferromagnetism, which takes advantage of proper Fermi surface (FS) nesting (or strong scattering) between different FS sheets [13, 14, 15, 16]; and 2) the frustrated Heisenberg exchange model of coupled magnetic moments of the localized d-orbital electrons around the Fe atoms [17, 18, 19, 20]. As for the itinerant electronic behavior, first principle band structure calculations [21] based on the density functional theory (DFT) indicate up to seven small Fermi pockets with three hole-like pockets centered around the  $\Gamma$  point and two electron-like ones centered around the  $M$  point of the folded Brillouin zone of the FeAs layers, which have partially supported by the angle-resolved photoemission spectroscopy (ARPES) from different groups [22, 23, 24, 25, 26]. Motivated by the DFT calculation and experimental measurements, in Refs. [15, 16], the excitonic mechanism [27] of itinerant carriers are employed taking account of the FS nesting between electron and hole pockets and the SDW phase are associated with triplet excitonic state, which can be understood as condensate of triplet electron-hole pairs

[27].

In this paper, we explore theoretically the effect of a single impurity on the local electronic structure of an Fe-based antiferromagnet in the triplet excitonic phase. It is shown that impurity bound states are formed inside the SDW gap, which may be observed experimentally by local probes. Before introducing the impurity, we first propose an effective model Hamiltonian to address the triplet excitonic state,

$$\begin{aligned} \hat{H}_{MF} = & \sum_{i,j,k} \sum_{\sigma} \psi_i(k) d_{ik}^{\sigma} d_{ik} \\ & + \sum_{k,X} \psi_X(k+X) c_{k+X}^{\dagger} c_{k+X} \\ & + \sum_{k,X} \sum_{i,j} \psi_i(k) d_{ik}^{\dagger} c_{k+X} + \text{H.c.}; \quad (1) \end{aligned}$$

where  $\psi = (0;0)$ ,  $X = (\pi;0)$ . We use the index  $i$  to label different valence bands around  $\Gamma$  point. Around  $X$  and  $Y$  points, there are two conduction bands.  $d_{ik}$  and  $c_{k+X}$  are the annihilation operators of electrons in the  $i$  and  $X$  bands. Theoretically  $X$  and  $Y$  are two equivalent nesting directions. Note that, the structural phase transition occurred just above/on the SDW transition breaks this equivalency. Without loss of generality, it is assumed that only conduction band around the  $X$  point couples with the valence bands around the  $\Gamma$  point, which is characterized by the mean-field order parameters  $\psi_i$ . For the triplet excitonic phase (SDW), we have real order parameters satisfying  $\psi_i^* = \psi_{i\#}$  and  $\psi_{i\#} = \psi_i = 0$  [27].

$\psi_i(k)$  and  $\psi_X(k)$  are used to denote the band dispersions of the nonmagnetic normal state. For  $k$  in the vicinity of the  $\Gamma$  point (therefore,  $k+X$  in the vicinity of the  $X$  point), the normal-state energy dispersions have ap-

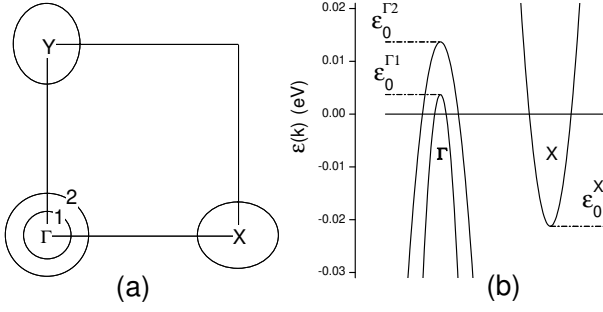


FIG. 1: Schematic plot of (a) the Fermi surfaces; and (b) the band dispersions of the valence (hole) band and conduction (electron) bands in the unfolded Brillouin Zone for the undoped parent compound. See text for detail.

proximately the 2D parabolic form as

$$\epsilon_1(\mathbf{k}) = \frac{\hbar^2(k_x^2 + k_y^2)}{2m_1} + \epsilon_0^1; \quad (2)$$

$$\epsilon_X(\mathbf{k} + \mathbf{X}) = \frac{\hbar^2(k_x^2 + k_y^2)}{2m_X} + \epsilon_0^X; \quad (3)$$

as schematically shown in Fig. 1. Here  $m_1$  and  $m_X$  are the corresponding effective masses. In describing the X band, the elliptic FS is approximated by the circular one for simplicity.  $\epsilon_0^1$  ( $\epsilon_0^X$ ) denotes the top (bottom) of the hole (electron) bands. According to the ARPES measurement [22], two hole-like Fermi pockets are revealed around the  $\Gamma$  point for undoped  $\text{BaFe}_2\text{As}_2$ . The band parameters extracted from the experimental data are as follows.  $m_1 = 2.8m_e$ ,  $m_2 = 7.4m_e$ , and  $m_X = 6.5m_e$ , where  $m_e$  is the mass of bare electron.  $\epsilon_0^1 = 4 \text{ meV}$ ,  $\epsilon_0^2 = 16 \text{ meV}$ , and  $\epsilon_0^X = 24 \text{ meV}$ . These parameters indicate that the nesting between the 2 band and X band is much better than that of the 1 band. Therefore it is natural to assume a larger order parameter  $\Delta_2$  and a vanishingly small  $\Delta_1$ . Let  $E_g = (\epsilon_0^2 + \epsilon_0^X)/2$  and  $\epsilon_0 = (\epsilon_0^2 - \epsilon_0^X)/2$ . Here  $E_g = 2E_g$  denotes the indirect gap between the top of the 2 band and the bottom of the X bands. Therefore,  $E_g > 0$  describes a semiconductor and  $E_g < 0$  a semiconductor. With the help of  $E_g$  and  $\epsilon_0$  and a further assumption of  $m_2 = m_X = m = 7m_e$ , we can re-express the energy dispersions as

$$\epsilon_2(\mathbf{k}) = \epsilon(\mathbf{k}) + \epsilon_0; \quad (4)$$

$$\epsilon_X(\mathbf{k} + \mathbf{X}) = \epsilon(\mathbf{k}) - \epsilon_0; \quad (5)$$

$$\epsilon(\mathbf{k}) = \frac{\hbar^2}{2m}k^2 - E_g; \quad (6)$$

Note that for  $\epsilon_0 = 0$ , the hole and electron bands are perfectly nested since  $\epsilon_2(\mathbf{k}) = \epsilon_X(\mathbf{k} + \mathbf{X})$  and the system is unstable with respect to infinitesimal Coulomb interaction while for nonzero  $\epsilon_0$  finite strength of Coulomb repulsion is needed.

For the reason that the order parameter  $\Delta_1$  is set to zero, there is no coupling between the 1 band and the X band. The Hamiltonian of Eq. (1) is reduced to a model of two bands with one valence band (2 band) and one conduction band (X band). Introducing the two-component Nambu operator,  $\hat{\psi}_{\mathbf{k}}^Y = (\hat{d}_{2\mathbf{k}}^Y; \hat{c}_{\mathbf{k}+\mathbf{X}}^Y)$ , the model Hamiltonian can be simplified as

$$\hat{H}_{MF} = \sum_{\mathbf{k}} \begin{pmatrix} \hat{\psi}_{\mathbf{k}}^Y \\ \hat{\psi}_{\mathbf{k}+\mathbf{X}}^Y \end{pmatrix} \begin{pmatrix} \epsilon_2(\mathbf{k}) & 0 \\ 0 & \epsilon_X(\mathbf{k} + \mathbf{X}) \end{pmatrix} \begin{pmatrix} \hat{\psi}_{\mathbf{k}}^Y \\ \hat{\psi}_{\mathbf{k}+\mathbf{X}}^Y \end{pmatrix} + H_{imp}; \quad (7)$$

where an impurity term has been added with the form,

$$\hat{H}_{imp} = \sum_{\mathbf{k}; k^0} \begin{pmatrix} \hat{\psi}_{\mathbf{k}; k^0}^Y \\ \hat{\psi}_{\mathbf{k}; k^0}^X \end{pmatrix} \hat{U}_{\mathbf{k}; k^0} \begin{pmatrix} \hat{\psi}_{\mathbf{k}; k^0}^Y \\ \hat{\psi}_{\mathbf{k}; k^0}^X \end{pmatrix}; \quad (8)$$

where  $\hat{U}_{\mathbf{k}; k^0}$  represents a  $2 \times 2$  matrix of the scattering potential associated with non-magnetic impurities. Here we use  $\hat{U}$  to denote  $\hat{U}_{\mathbf{k}; k^0}$  for short. The Green's function method is applied to study the single impurity effect. The matrix Green's functions are defined as

$$\hat{G}(\mathbf{k}; i; k^0; 0) = \frac{1}{Z} \text{Tr} [\hat{G}(\mathbf{k}; i; k^0; 0)]; \quad (9)$$

$$\hat{G}(\mathbf{k}; k^0; i; n) = \frac{1}{Z} \text{Tr} [\hat{G}(\mathbf{k}; k^0; 0) e^{i\tau_n}]; \quad (10)$$

$$\hat{G}(\mathbf{k}; k^0; i) = \hat{G}(\mathbf{k}; k^0; i; n \rightarrow \infty + i0^+); \quad (11)$$

From the Hamiltonian defined in Eq. (7) we can derive the bare Green's function

$$\hat{G}^0(\mathbf{k}; i) = \begin{pmatrix} \epsilon_2(\mathbf{k}) & 0 \\ 0 & \epsilon_X(\mathbf{k} + \mathbf{X}) \end{pmatrix}^{-1}; \quad (12)$$

$$= \frac{1}{2} \begin{pmatrix} \hat{\sigma}_0 + \hat{\sigma}_1 & 0 \\ 0 & \hat{\sigma}_0 - \hat{\sigma}_1 \end{pmatrix} \frac{1}{\epsilon(\mathbf{k}) \mp E_g}; \quad (13)$$

where  $\hat{\sigma}_i = \hat{\sigma}_i + \hat{\sigma}_0$ ,  $\hat{\sigma}_0$  is the  $2 \times 2$  unit matrix, and  $\hat{\sigma}_{1,3}$  are the Pauli matrices. The T-matrix approximation is employed to compute the Green's function in the presence of impurities. For a single impurity, the T-matrix exactly accounts for the multiple scattering of the impurity. The single-particle Green's function  $\hat{G}$  can be obtained from the following Dyson's equation,

$$\hat{G}(\mathbf{k}; k^0; i) = \hat{G}^0(\mathbf{k}; i) + \hat{G}^0(\mathbf{k}; i) \hat{T}(\mathbf{k}; k^0; i) \hat{G}^0(\mathbf{k}; i); \quad (14)$$

where the T-matrix is given by

$$\hat{T}(\mathbf{k}; k^0; i) = \hat{U}_{\mathbf{k}; k^0} + \sum_{\mathbf{k}''} \hat{U}_{\mathbf{k}; k^0} \hat{G}^0(\mathbf{k}'') \hat{T}(\mathbf{k}'') \hat{G}^0(\mathbf{k}; k^0; i); \quad (15)$$

For a point-like scattering potential interacting with itinerant carriers just on the impurity site, the scattering matrix is isotropic,  $\hat{U}_{\mathbf{k}; k^0} = \hat{U}$ . The above equation is greatly simplified

$$\hat{T}(\mathbf{k}; i) = \hat{U} + \hat{U} \hat{G}^0(\mathbf{k}; i) \hat{T}(\mathbf{k}; i); \quad (16)$$



Substituting Eq. (27) into Eq. (26) we may single out the variation of LDOS due to the presence of the impurity potential,

$$N_{\text{imp}}(r; \epsilon) = \frac{1}{\pi} \text{Im} \text{Tr} [\hat{G}^0(r; 0; \epsilon) \hat{V}(\epsilon)] \quad (28)$$

For the second impurity model [30], Fig. 2 (a) shows the LDOS as a function of energy  $\epsilon$  on the impurity site, namely  $N(0; \epsilon)$ , while Fig. 2 (b) the impurity-induced LDOS at the bound energy as a function of radial distance  $r$  on the impurity site, i.e.  $N_{\text{imp}}(r; \epsilon)$ .  $V_{\text{imp}}$  has been set as -0.36, -0.6, and -4.0 eV, giving rise to the impurity bound states seen as the sharp peaks located respectively at the energies  $\epsilon = 0, 0.5$ , and  $0.99$  in Fig. 2 (a). The probability densities of these bound states exhibit a kind of exponential decay with the Friedel oscillation, as seen in Fig. 2 (b). Introducing two length scales,  $\lambda_1$  and  $\lambda_2$  to characterize the oscillation and decay, we obtain the asymptotic behavior of  $N_{\text{imp}}(r; \epsilon)$  for large  $r$ ,

$N_{\text{imp}}(r; \epsilon) / r^{-1} \cos^2(r/\lambda_1) \exp(-r/\lambda_2)$ : (29)  
 $\lambda_1 = a = \frac{\pi}{4 N_0 E_g}$  which is approximately 5.7 in consistency with the numerical results shown in Fig. 2 (b).  
 $\lambda_2 = 1/E_g = (\frac{\pi^2}{2} \epsilon^2)^{-1/2} = 0.32, 0.37$ , and  $2.3$  for the three cases of impurity states. This explains why we see clear Friedel oscillation for impurity state with bound energy near the gap edge.

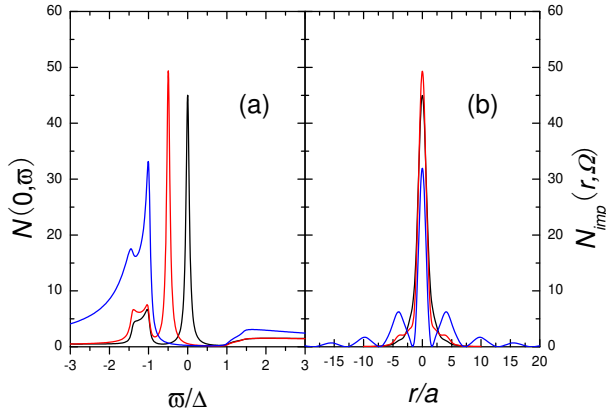


FIG. 2: LDOS on the impurity site as a function of energy  $\epsilon$ , i.e.  $N(0; \epsilon)$  (a), and impurity-induced LDOS at the bound energy  $\epsilon$  as a function of radial distance  $r$  on the impurity site, i.e.  $N_{\text{imp}}(r; \epsilon)$  (b).  $r$  is in unit of  $a$  with  $a$  the lattice constant of Fe-Fe plane. Black, red, and blue lines correspond to  $V_{\text{imp}} = -0.36; -0.6; -4$  eV, respectively.

This work was supported by the NSFC grant under Grants Nos. 10674179 and 10429401, the GRF grant of Hong Kong.

- [2] C. de la Cruz et al, Nature 453, 899 (2008); J. Zhao et al., arXiv:0806.2528; J. Zhao et al., arXiv:0807.1077.
- [3] Y. Chen et al, Phys. Rev. B 78, 064515 (2008), see also arXiv.org:0806.0662.
- [4] Q. Huang et al, arXiv:0806.2776.
- [5] M. A. McGuire et al, arXiv.org:0806.3878.
- [6] A. A. Czele et al, arXiv:0807.1044.
- [7] A. I. Goldman et al, arXiv.org:0807.1525.
- [8] H. Takahashi et al, Nature 453, 376 (2008).
- [9] Z.-A. Ren et al, Europhys. Lett. 82, 57002 (2008).
- [10] H. H. Wen et al, Europhys. Lett. 82, 17009 (2008), see also arXiv:0803.3021.
- [11] X. H. Chen et al, Nature 453, 761 (2008), see also arXiv:0803.3603.
- [12] G. F. Chen et al, Phys. Rev. Lett. 100, 247002 (2008), see also arXiv:0803.3790.
- [13] J. Dong et al, Europhys. Lett., 83, 27006 (2008); see also arXiv:0803.3426.
- [14] I. I. Mazin et al, Phys. Rev. Lett. 101, 057003 (2008), see also arXiv:0803.2740; arXiv.org:0806.1869.
- [15] Q. Han, Y. Chen, and Z. D. Wang, Europhys. Lett. 82, 37007 (2008), see also arXiv:0803.4346.
- [16] V. Barzykin and L. P. Gor'kov, arXiv:0806.1933.
- [17] T. Yildirim, Phys. Rev. Lett. 101, 057010 (2008), see also arXiv:0804.2252.
- [18] Q. Si and E. Abraham, arXiv:0804.2480.
- [19] F. J. Ma, Z. Y. Li, and T. Xiang, arXiv.org:0804.3370.
- [20] C. Fang et al, Phys. Rev. B 77, 224509 (2008), see also arXiv:0804.3843.
- [21] D. J. Singh and M. H. Du, Phys. Rev. Lett. 100, 237003 (2008), see also arXiv:0803.0429; G. Xu et al, Europhys. Lett., 82, 67002 (2008), see also arXiv:0803.1282; K. Haule, J. H. Shim and G. Kotliar, Phys. Rev. Lett. 100, 226402 (2008), see also arXiv:0803.1279; F. Ma, and Z.-Y. Lu, Phys. Rev. B 78, 033111 (2008), see also arXiv:0803.3286; I. A. Nekrasov, Z. V. Pchelkina, M. V. Sadovskii, JETP Lett., 88, 144 (2008), see also arXiv:0806.2630; F. Ma, Z.-Y. Lu, and T. Xiang, arXiv:0806.3526; D. J. Singh, arXiv:0807.2643.
- [22] L. X. Yang et al, arXiv:0806.2627.
- [23] C. Liu et al, arXiv:0806.3453.
- [24] L. Zhao et al, arXiv:0807.0398.
- [25] H. Ding et al, Europhys. Lett. 83, 47001 (2008), see also arXiv:0807.0419; P. Richard et al, arXiv:0808.1809.
- [26] D. H. Lu et al, arXiv:0807.2009.
- [27] B. I. Halperin and T. M. Rice, Solid State Phys. 21, 125 (1968).
- [28] J. Zittartz, Phys. Rev. 164, 575 (1967).
- [29] The impurity Hamiltonian is expressed as  $H_{\text{imp}} = \int U_{\text{imp}}(r) \psi^\dagger(r) \psi(r) dr = \sum_{k, k_0} \hat{c}_{k, k_0}^\dagger \hat{c}_{k, k_0}$  where  $\hat{c}_{k, k_0}^\dagger = (\hat{c}_k^\dagger; \hat{c}_{k+k_0}^\dagger)$ ,  $\psi(r) = 2^{-1/2} \sum_k \hat{c}_k(r) d_k + \hat{c}_{k+k_0}(r) c_{k+k_0}$ , with  $\hat{c}_k(r)$  and  $\hat{c}_{k+k_0}(r)$  Bloch functions of quasimomentum  $k$ . In this paper the scattering potential is assumed to be pointlike,  $U_{\text{imp}} = V_{\text{imp}}(r)$ . With further simplification of the Bloch functions of the form  $\exp(ik \cdot r)$ ,  $\hat{c}_{k, k_0}$  is  $k$  independent and equal to  $V_{\text{imp}}(\hat{\epsilon}_0 + \hat{\epsilon}_1) = 2$ .
- [30] The following conclusions are also qualitatively correct for the first impurity model.